Biogeosciences Discuss., 12, 16313–16357, 2015
www.biogeosciences-discuss.net/12/16313/2015/
doi:10.5194/bgd-12-16313-2015

Biogeosciences
Discussions
Open Access

Coupling carbon allocation with leaf and root phenology predicts tree-grass partitioning along a savanna rainfall gradient

V. Haverd[1], B. Smith[2], M. Raupach[3,†], P. Briggs[1], L. Nieradzik[1], J. Beringer[4], L. Hutley[5], C. M. Trudinger[6], and J. Cleverly[7]

[1]CSIRO Oceans and Atmosphere, P.O. Box 3023, Canberra ACT 2601, Australia
[2]Lund University, Department of Physical Geography and Ecosystem Science, 223 62 Lund, Sweden
[3]Australian National University, Climate Change Institute, Canberra, ACT 0200, Australia
[4]School of Earth and Environment, The University of Western Australia, M004. 35 Stirling Highway, Crawley, WA, 6009, Australia
[5]Research Institute for the Environment and Livelihoods, Charles Darwin University, NT, 0909, Australia
[6]CSIRO Oceans and Atmosphere, PMB 1 Aspendale, Vic 3195, Australia
[7]School of Life Sciences, University of Technology, Sydney, P.O. Box 123, Broadway NSW, 2007, Australia
[†]deceased

Received: 24 August 2015 – Accepted: 31 August 2015 – Published: 5 October 2015

Correspondence to: V. Haverd (vanessa.haverd@csiro.au)

Published by Copernicus Publications on behalf of the European Geosciences Union.

Abstract

The relative complexity of the mechanisms underlying savanna ecosystem dynamics, in comparison to other biomes such as temperate and tropical forests, challenges the representation of such dynamics in ecosystem and Earth system models. A realistic representation of processes governing carbon allocation and phenology for the two defining elements of savanna vegetation (namely trees and grasses) may be a key to understanding variations in tree/grass partitioning in time and space across the savanna biome worldwide. Here we present a new approach for modelling coupled phenology and carbon allocation, applied to competing tree and grass plant functional types. The approach accounts for a temporal shift between assimilation and growth, mediated by a labile carbohydrate store. This is combined with a method to maximise long-term net primary production (NPP) by optimally partitioning plant growth between fine roots and (leaves + stem). The computational efficiency of the analytic method used here allows it to be uniquely and readily applied at regional scale, as required, for example, within the framework of a global biogeochemical model.

We demonstrate the approach by encoding it in a new simple carbon/water cycle model that we call HAVANA (Hydrology and Vegetation-dynamics Algorithm for Northern Australia), coupled to the existing POP (Population Orders Physiology) model for tree demography and disturbance-mediated heterogeneity. HAVANA-POP is calibrated using monthly remotely-sensed fraction of absorbed photosynthetically active radiation (fPAR) and eddy-covariance-based estimates of carbon and water fluxes at 5 tower sites along the Northern Australian Tropical Transect (NATT), which is characterized by large gradients in rainfall and wildfire disturbance. The calibrated model replicates observed gradients of fPAR, tree leaf area index, basal area and foliage projective cover along the NATT. The model behaviour emerges from complex feed-backs between the plant physiology and vegetation dynamics, mediated by shifting above- vs. below-ground resources, and not from imposed hypotheses about the controls on tree/grass co-existence. Results support the hypothesis that resource limitation is a stronger determinant of tree cover than disturbance in Australian savannas.

1 Introduction

Savannas constitute one of the world's most extensive biomes and provide ecosystem services as rangelands and marginal agricultural lands for one-fifth of the world's population (Lehmann et al., 2009). Being sensitive to variations in rainfall and water availability, they have a primary role in governing interannual variability in biosphere–atmosphere carbon exchange and the CO_2 concentration of the atmosphere (Ahlström et al., 2015; Poulter et al., 2014). For the last three decades, semi-arid ecosystems (including savannas) globally have exhibited a positive net carbon uptake trend (Ahlström et al., 2015), coinciding with regional observations of woody encroachment and increased vegetation greenness when viewed from space (Donohue et al., 2009; Liu et al., 2015). The biogeochemical dynamics of seasonally dry savannas are modulated by stress tolerance and pulse response behaviour of the drought adapted biota as the environment shifts seasonally in the relative availability of above- (light) and below-ground (mainly water) resources. Resource competition – or avoidance of competition through spatial and temporal niche segregation (Ward et al., 2013) – between trees and grasses, as well as disturbances due to grazing animals and fires (Lehmann et al., 2014; Sankaran et al., 2005) drives shifts in allocation and tree vs. grass performance that feed back to and tightly couple the water and carbon cycles. The relative complexity of the mechanisms underlying savanna ecosystem dynamics, in comparison to other biomes such as temperate and tropical forests, challenges the representation of such dynamics in ecosystem and Earth system models (Baudena et al., 2015).

Phenology and allocation of carbon to leaves, roots and stems are critical determinants of savanna productivity (Ma et al., 2013; Scholes and Walker, 2004). Savanna vegetation occurs in regions of high rainfall variability and, while vegetation is often water-limited, light can limit production seasonally or during heavy precipitation

episodes (Whitley et al., 2011). Species may partition available carbon seasonally and interannually in order to optimise uptake of variably available resources above and below ground. Resource availability often changes quickly: species respond by producing resource uptake surfaces quickly to optimise uptake of the most limiting resource – leaves to capture light when soil water is abundant, fine roots to increase water uptake as supplies deplete. To enable a rapid response to changing resources, plants draw on stored non-structural carbohydrates (NSC) in storage, which are accumulated during times of plenty. This must lead to a temporal shift between plant growth and carbon capture.

A realistic representation of processes governing carbon allocation and phenology for the defining elements of savanna vegetation (namely trees and grasses) may thus be a key to understanding variations in tree/grass partitioning in time and space in the savanna biome worldwide. Global vegetation models typically treat allocation and phenology as independent processes. One exception is the ADGVM model of Scheiter and Higgins (2009) which is specialised for the simulation of savannas. It uses an individual plant's carbon status to determine the transition between active and dormant states, dynamically allocating carbon based on resource (light or water) limitation. However, no large-scale vegetation model of which we are aware allows phenology to emerge as a result of allocation of assimilated carbon to leaves and roots in response to changing relative availability of above- and below-ground resources during the course of a growing season or between years.

Here we present a new approach that links phenology and allocation, accounting for a temporal shift between assimilation and growth, which is mediated by a labile carbohydrate store. The novelty of the approach lies in the dynamic constraint of plant growth such that the long term change in store (net primary production minus growth) is zero (a requirement for carbon conservation). This is combined with the use of an optimal response method for analytically predicting the partitioning of plant growth between fine roots and (leaves + stem), which optimises long term NPP. While optimal response methods for carbon allocation are not new (Franklin et al., 2012), and have

been applied to savanna vegetation (Schymanski et al., 2009) the computational efficiency of the analytic method used here allows it to be uniquely readily applied at regional scale, as required, for example, within the framework of a land surface model or ESM.

We demonstrate the approach by encoding it in a simple carbon/water cycle model that we call HAVANA (Hydrology and Vegetation-dynamics Algorithm for Northern Australia), coupled to the POP (Population Orders Physiology) model for tree demography and disturbance-mediated heterogeneity (Haverd et al., 2013b, 2014). HAVANA-POP is applied to and tested against observations from the Northern Australian Tropical Transect, featuring gradients in rainfall and wildfire disturbance. In particular, the model is evaluated against a suite of observations that are sensitive to the tree-grass ratio along the transect, namely: eddy-covariance-based estimates of carbon and water fluxes at 5 tower sites; dynamics of remotely-sensed fPAR; tree leaf area index derived from digital hemispheric photography and satellite observations; gradients of tree basal area and foliage projective cover.

2 Model description

HAVANA is a new model of landscape water balance and plant function. It contains two water stores (upper and lower soil) and leaf and fine root compartments for each of two competing vegetation types: trees and grass. The tree vegetation type also has a stem compartment, which includes coarse roots. The stem compartment is partitioned between sapwood and heartwood via coupling to the POP module (Haverd et al., 2013b), which accounts for tree demography and landscape-heterogeneity mediated by disturbance.

Qualitative relationships between key variables for a single vegetation type (trees) are shown in Fig. 1. The schematic also applies to grass, except that the stem component does not apply in grasses, and grass fine-roots do not access the deep soil

moisture store. Although not represented in Fig. 1, trees and grass interact via competition for water in the shallow upper soil layer, and competition for light.

In the model, soil water stores change in response to input from precipitation and losses due to evapotranspiration, deep drainage and surface runoff (Fig. 1). Dynamics of vegetation carbon stores are governed by growth and turnover rates. Growth is constrained to be equal to net primary production (NPP, equal to gross primary production minus autotrophic respiration) in the long term, but is temporally dependent on the size of the NSC store, soil water availability and the deviation of the structural carbon store from an internally computed carbon carrying capacity, above which growth stops and NPP is stored away as NSC. Growth is partitioned between (leaf + stem) and fine root compartments using an optimal response theory in which long term NPP is the fitness proxy. That is, we assume the ecological optimality hypothesis, that evolutionary selection pressures drive ecosystems towards maximal utilization of available resources for the production of biomass, so that long-term NPP over many reproductive cycles takes the largest possible value under the constraints of available resources (Raupach, 2005). This leads to a negative feed-back of soil moisture on allocation to fine roots, in favour of the combined (leaf + stem) compartment. Partitioning of growth between leaf and stem is influenced by the relative magnitudes of leaf and sapwood compartments, which are constrained by the Pipe Model (Shinozaki et al., 1964), in which sapwood cross-sectional area is assumed to be a constant proportion of total leaf area. Leaf and fine root carbon stores are subject to first order decay, while turnover of woody biomass is given by the mortality (both resource-limitation and disturbance components, including fire) computed within the POP module (Sect. 2.3 and Appendix A).

The carbon and water cycles are primarily linked by the transpiration component of evapotranspiration, with a secondary link being the dependences of growth and growth-partitioning on soil moisture. Transpiration, equivalent to root water extraction, is modelled as the lesser of evaporative demand (dependent on radiation, air temperature and fraction cover) and supply-limited root water uptake, which depends both on soil moisture and root density in each soil layer.

Trees and grass compete for light and water. Tree roots can potentially access water in both shallow and deep soil layers, whereas grass roots are assumed unable to access the deep soil moisture store. Further, grass is partially shaded by trees as a function of tree cover.

A quantitative description of the model follows. All parameter symbols, meaning, values and sources are listed in Table 1.

2.1 Water balance model

The water balance model is that of the Australian Water Availability Project (Raupach. et al., 2009), with modification to the transpiration terms to allow for root-carbon dependence, and is described here in full for completeness.

State variables: The two state variables of the water balance model are soil water stores (W_1, W_2) [m water] corresponding to upper and lower soil layers. The layers together encompass the whole soil profile from which water is extracted by plant transpiration. Corresponding dimensionless variables are the relative soil water (w_1, w_2) in the two stores, between 0 and 1 and related to W_1 and W_2 by

$$w_i = W_i/(\theta_{S_i} Z_{W_i}) \quad (i = 1,2) \tag{1}$$

where θ_{S_i} [$m^3\,m^{-3}$] is the saturated volumetric water content and Z_{W_i} [m] is the thickness of layer i.

Balance equations: The dynamic equations governing W_1 and W_2 are the mass conservation equations for soil water:

$$\begin{aligned}
\frac{dW_1}{dt} = \theta_{S_1} Z_{W_1} \frac{dw_1}{dt} &= \underset{\text{Precipitation}}{F_{\text{WPrec}}} - \underset{\substack{\text{Transpiration}\\ \text{from layer 1}}}{F_{\text{WTra1}}} - \underset{\substack{\text{Soil}\\ \text{Evaporation}}}{F_{\text{WSoil}}} - \underset{\substack{\text{Surface}\\ \text{Runoff}}}{F_{\text{WRun}}} - \underset{\substack{\text{Leaching from}\\ \text{layer 1 to 2}}}{F_{\text{WLch1}}} \\
\frac{dW_2}{dt} = \theta_{S_2} Z_{W_2} \frac{dw_2}{dt} &= \underset{\substack{\text{Leaching from}\\ \text{layer 1 to 2}}}{F_{\text{WLch1}}} - \underset{\substack{\text{Deep}\\ \text{Drainage}}}{F_{\text{WLch2}}} - \underset{\substack{\text{Transpiration}\\ \text{from layer 2}}}{F_{\text{WTra2}}}
\end{aligned} \tag{2}$$

where all water fluxes (F_W) are in metres of water per day [m H_2O d^{-1}].

Phenomenological equations: The phenomenological equations for water fluxes are as follows.

(1) *Precipitation* (F_{WPrec}) is an external input.

(2) *Transpiration* (F_{WTra}) is defined for each soil layer ($i = 1,2$) and each plant type (j = grass [g], trees [wood = w]) as the lesser of an energy-limited transpiration rate $F_{WTra(ELim),j}$ and a water-limited transpiration rate $F_{WTra(WLim),j}$:

$$F_{WTra,i,j} = \min(F_{WTra(ELim)i,j},\ F_{WTra(WLim)i,j}) \quad (3)$$

(Note here that $F_{WTra,2,grass} = 0$, as it is assumed that grass roots do not access the lower soil moisture store.)

The total energy-limited transpiration rate (summed over two soil layers) is partitioned among soil layers using the water-limited transpiration for each layer under prevailing (energy-limited) conditions, so that:

$$F_{WTra(Elim)i,j} = F_{WTra(Elim)j}[F_{WTra(Wlim)i,j}/(F_{WTra(Wlim)1,j} + F_{WTra(Wlim)2,j})] \quad (4)$$

The total energy-limited transpiration rate, $F_{WTra(ELim)}$, and the water-limited transpiration for each layer, $F_{WTra(WLim)i}$, are defined as follows.

The total energy-limited transpiration rate is the evaporation rate from the surface without soil water constraints. It is often defined using the Penman–Monteith equation, but for reasons of both physics (Raupach, 2001, 2000) and simplicity, it is defined here as

$$F_{WTra(ELim),j} = v_j F_{W(PT)} \quad (5)$$

where v_j is the tree or grass vegetation cover fraction and $F_{W(PT)}$ is the Priestley–Taylor evaporation rate [m H_2O d^{-1}], a thermodynamic estimate of the energy-limited evaporation rate for the whole surface (vegetation plus soil). The factor v_j relates energy-limited total evaporation to the plant component only.

From Raupach (2000, 2001), $F_{W(PT)}$ is

$$F_{W(PT)} = c_{PT}\Phi_{Eq}/(\rho_W \lambda_W) \quad (6)$$

where ρ_W [mol H_2O m^{-3}] is the density of liquid water, λ_W [J mol H_2O^{-1}] is the latent heat of vaporisation of water, Φ_{Eq} [J m^{-2} d^{-1}] is the thermodynamic equilibrium latent heat flux, and c_{PT} is the Priestley–Taylor coefficient, a number which is well constrained at about 1.26 (Priestley and Taylor, 1972; Raupach, 2001). The equilibrium latent heat flux is given by

$$\Phi_{Eq} = p\varepsilon\Phi^*_A/(p\varepsilon + 1) \quad (7)$$

where Φ^*_A is the isothermal available energy flux, ε is the ratio of latent to sensible heat content of saturated air (2.2 at 20 °C, roughly doubling with each 13 °C temperature increase) and p is a number slightly less than 1 accounting for radiative coupling:

$$p = \frac{G_a}{G_a + G_r} \quad (8)$$

where G_a is the aerodynamic conductance for heat and water vapour transfer; $G_r = 4e\sigma T_a^3/(\rho_A c_{PA})$ is the radiative conductance; ρ_A [mol m^{-3}] is the density of air; and c_{PA} is the specific heat of air at constant pressure [J mol^{-1} K^{-1}].

The isothermal available energy flux Φ^*_A is given by

$$\Phi^*_A = (1 - a)\Phi_{S\downarrow} + e(\Phi_{L\downarrow} - \sigma T_a^4) \quad (9)$$

where $\Phi_{S\downarrow}$ and $\Phi_{L\downarrow}$ are the downward solar (shortwave) and thermal (longwave) irradiances; a and e are whole-surface albedo and emissivity, respectively; σ is the Stefan–Boltzmann constant; T_a [K] is the air temperature at a reference height.

Energy fluxes (Φ) are calculated as averages over daylight hours only, since it is assumed that total evaporation ($F_{WE} = F_{WTra} + F_{WSoil}$) and its components are all zero at

night. Downward daytime longwave irradiance is estimated with the Swinbank (1963), formula:

$$\Phi_{L\downarrow} = 335.97(T_a/293)^{6.0} \quad (10)$$

using average daytime T_a estimated as $0.75T_{a,max} + 0.25T_{a,min}$.

The water-limited transpiration rate in layer i by plant type j is parameterised as:

$$F_{WTra(WLim)i,j} = k_{E,i,j}C_{R,i,j}w_i^{p_{extract}} \quad (11)$$

where $k_{E,i,j}$ is a rate per unit root carbon density [$m\,d^{-1}\,(mol\,C\,m^{-2})^{-1}$] for the uptake of water by roots from a drying soil under water-limited transpiration, and $C_{R,i,j}$ is the root carbon density [$mol\,C\,m^{-2}$] of soil layer i and plant type j.

(3) *Soil evaporation* (F_{WSoil}) is formulated as:

$$F_{WSoil} = (1 - v)w_1^{\beta}F_{W(PT)} \quad (12)$$

where β is an exponent specifying the response of soil evaporation to upper-layer soil water (w_1).

(4) *Surface runoff* (F_{WRun}) is given by

$$F_{WRun} = F_{WPrec}\,\mathrm{Step}(w_1 - 1) \quad (13)$$

All precipitation runs off when the upper-layer soil is saturated, and there is no runoff otherwise.

(5) *Leaching* (F_{WLch}) or drainage downward out of soil layer i is given by

$$F_{WLch,\,i} = K_{S,\,i}w_i^{\gamma} \quad (14)$$

where γ is an exponent specifying the response of drainage to relative soil water w_i, and $K_{S,\,i}$ [$m\,d^{-1}$] is the saturated hydraulic conductivity of soil layer i.

2.2 Model of vegetation function

State variables and governing equations: The state variables of the vegetation model are carbon pools in leaves and fine roots of trees and grass, and the woody carbon pool (stem plus coarse roots) in trees. The dynamics of these pools are governed by their mass conservation equations, with each pool augmented by a proportion a of the growth flux. Leaf and fine root pools are depleted by first order decay, while all tree carbon pools are depleted by tree mortality:

$$\frac{dC_{L,j}}{dt} = \alpha_{L,j}F_{C,Growth,j} - k_{L,j}C_{L,j} - \frac{C_{L,j}}{C_{stem}}m_{stem,j} \quad (15)$$

$$\frac{dC_{R,i,j}}{dt} = \alpha_{R,i,j}F_{C,Growth,j} - k_{R,j}C_{R,i,j} - \frac{C_{R,i,j}}{C_{stem}}m_{stem,j} \quad (16)$$

$$\frac{dC_{stem}}{dt} = \alpha_{stem}F_{C,Growth,w} - m_{stem} \quad (17)$$

In Eqs. (15)–(17), C denotes a carbon pool [$mol\,C\,m^{-2}$]; α a carbon allocation coefficient; L leaves; R fine roots; stem trunk plus coarse roots k a first order rate constant [d^{-1}]; j a plant type (woody or grassy) and i a soil layer (upper or lower), $m_{stem,j}$ is stem biomass turnover [$mol\,C\,m^{-2}\,d^{-1}$], which is zero for grass, and computed by POP for trees (See Sect. 2.3).

For woody vegetation, we adopt a dependence of leaf turnover on specific leaf area, based on the synthesis of Wright et al. (2002):

$$k_{L,w} = 1/\left(365\left(\frac{A_{SL,w}}{60}\right)^{-1.2}\right) \quad (18)$$

2.2.1 Growth

Growth (the flux of carbon to structural components) is parameterised by a logistic curve, inspired by Choler et al. (2010), who specified growth of grasses in water-

controlled ecosystems as the product of (i) a growth scaling parameter, (ii) relative soil moisture content, (iii) one minus current leaf carbon, relative to a fixed carrying capacity and (iv) current leaf carbon

In contrast we specify growth following Eq. (19) as the product of: (i) a growth scaling parameter (β_{growth}), (ii) $f_{\text{w},j}$, an increasing function of soil water in the upper soil layer (grass) or lower soil layer (trees) (Eq. 20) (n.b. that trees and grass nonetheless compete for water in the upper soil layer via transpiration) (iii) one minus (leaf + fine root) carbon relative to a prognostic carrying capacity $C_{\text{max},j}$, above which growth stops and net primary production is stored away as non-structural carbohydrate, (iv) the sum of (a) long-term NPP, (b) a multiple of the long-term net flux (NPP – growth) to the NSC store, and (c) a residual component $F_{0,\text{growth}}$, allowing regrowth to occur, should the plant C stores decline to zero.

$$F_{\text{C,Growth},j} = \beta_{\text{growth}} f_{\text{w},j} \max\left[\left(1 - \frac{C_{\text{leaf},j} + \sum_i C_{\text{R},i,j}}{C_{\text{max},j}}\right), 0.0\right] \left(F_{0,\text{growth}} + \max\left[\overline{F_{\text{C,NPP},j}} + k_{\text{store}}\left(\overline{F_{\text{C,NPP},j}} - \overline{F_{\text{C,growth},j}}\right), 0.0\right]\right) \quad (19)$$

$$f_w = \frac{1 - \left(1 + \left(\frac{\text{w}}{\text{w}_{\text{thresh}}}\right)^{p_{\text{growth}}}\right)^{-1}}{1 - \left(1 + \left(\frac{1}{\text{w}_{\text{thresh}}}\right)^{p_{\text{growth}}}\right)^{-1}} \quad (20)$$

2.2.2 Dynamic storage (coupling of net primary production and growth)

Growth is constrained to equal time-averaged NPP over some averaging period ($t_{\text{av},j}$) (set here to 1 yr for grass and 3 yr for trees), producing a change in storage of carbohydrate (NPP minus Growth) which averages to zero. This is achieved by adjusting $C_{\text{max},j}$

dynamically according to:

$$\frac{\text{d}C_{\text{max},j}}{\text{d}t} = \begin{cases} K_{\text{growth}}\left(\frac{\overline{F_{CNPP,j}} - \overline{F_{\text{C,Growth},j}}}{\overline{F_{\text{C,Growth},j}}}\right)^2 \left(\frac{C_{\text{leaf},j} + \sum_i C_{\text{R},i,j}}{C_{\text{max}}}\right) \left(C_{\text{leaf},j} + \sum_i C_{\text{R},i,j}\right); \\ \overline{F_{CNPP,j}} - \overline{F_{\text{C,Growth},j}} > 0 \\ -K_{\text{growth}}\left(\frac{\overline{F_{CNPP,j}} - \overline{F_{\text{C,Growth},j}}}{\overline{F_{\text{C,Growth},j}}}\right)^2 \left(\frac{C_{\text{leaf},j} + \sum_i C_{\text{R},i,j}}{C_{\text{max}}}\right)^{-1} \left(C_{\text{leaf},j} + \sum_i C_{\text{R},i,j}\right); \\ \overline{F_{\text{CNPP},j}} - \overline{F_{\text{C,Growth},j}} \le 0 \end{cases} \quad (21)$$

Such that $C_{\text{max},j}$ increases if time-averaged net primary production exceeds growth and decreases otherwise. $C_{\text{max},j}$ is maintained above C_0.

2.2.3 Net Primary Production

Net primary production is the difference between gross primary production ($F_{\text{C,GPP},j}$) and maintenance respiration of leaves and fine roots, scaled by ($1 - c_{\text{growth}}$) to account for growth respiration (Ryan, 1991):

$$F_{\text{C,NPP},j} = (1 - c_{\text{growth}})\left(F_{\text{C,GPP},j} - \sum_i F_{\text{C,R}m,\text{R},i,j} - F_{\text{C,R}m,\text{L},j} - F_{\text{C,R}m,w}\right) \quad (22)$$

2.2.4 Gross Primary Production

Plant gross primary production ($F_{\text{C,GPP},j}$) is evaluated as the lesser of light- and water-limited components:

$$F_{\text{C,GPP},j} = \min[(\alpha_{\text{Q},j} v_j F_{\text{Q}}), (\alpha_{\text{W}} \rho_{\text{W}} F_{\text{WTra},j})] \quad (23)$$

where F_{Q} is the incident quantum flux of photosynthetically active radiation (PAR) on the surface [mol quanta $\text{m}^{-2}\,\text{d}^{-1}$], and α_{Q} and α_{W} are respectively a PAR use efficiency

[mol C mol quanta^{-1}] and a transpired-water use efficiency [mol C mol H_2O^{-1}]. Of these, α_Q is a prescribed parameter, and α_W is calculated as

$$\alpha_W = m_{\alpha,j}([CO_2]_a - [CO_2]_c)/(1.6D_S) \quad (24)$$

where $m_{\alpha,j}$ is a dimensionless multiplier, $[CO_2]_a$ is the atmospheric CO_2 concentration, $[CO_2]_c$ is the CO_2 compensation point [molC molAir^{-1}] calculated using the (Von Caemmerer, 2000) algorithm:

$$[CO_2]_c = 37.0 \times 10^{-6} \times 1.37^{\frac{T_S - 25.0}{10.0}} \quad (25)$$

D_S is the surface saturation deficit [mol H_2O^{-1} mol Air^{-1}], calculated from the air saturation deficit D_a as in (Raupach, 1998):

$$D_S = D_a + \frac{\varepsilon\,(p\,(\Phi_A - \Phi_E)) - \Phi_E}{\rho_A c_p G_a} \quad (26)$$

and surface temperature T_S is given by:

$$T_S = T_a + \frac{\varepsilon\,(p\,(\Phi_A - \Phi_E))}{\rho_A c_p G_a} \quad (27)$$

2.2.5 Maintenance respiration

The rate of maintenance respiration for the jth compartment (sapwood, leaf or fine roots) is formulated as:

$$R_{m,j} = k_{resp} C_j / \text{ratio}_{CtoN,j}\, g(T_a) \quad (28)$$

where $k_{resp} = 0.0548\,\text{d}^{-1}$ is the rate constant for maintenance respiration (Sprugel et al., 1995), and $g(T)$ is the ecosystem respiration temperature response function

of Lloyd and Taylor (1994) adopted by Sitch et al. (2003) in the LPJ model:

$$g(T) = \exp\left[308.56\left(\frac{1}{56.02} - \frac{1}{T - 227.13}\right)\right] \quad (29)$$

and ratio_{CtoN} is the mass ratio of carbon to nitrogen in the plant tissue, here taken as 30 for leaves and fine roots, and 300 for sapwood.

2.2.6 Carbon allocation

Following Raupach (2005), we choose time-dependent carbon allocation coefficients to maximise the total carbon gain, namely the long-term integral of $F_{C,NPP,j}$ for each plant type. As discussed by Raupach (2005), the vector of allocation coefficients has "bang-bang" character, meaning that, at each instant t, an allocation coefficient of one is assigned to the pool for which the marginal return on invested growth is largest while all the other pools receive zero allocation:

$$\alpha_{L,j} + \alpha_{stem,j} = H\left[\frac{\delta F_{C,NPP,j}}{\delta C_{L,j}} - \frac{\delta F_{C,NPP,j}}{\delta C_{R,1,j}}\right] H\left[\frac{\delta F_{C,NPP,j}}{\delta C_{L,j}} - \frac{\delta F_{C,NPP,j}}{\delta C_{R,2,j}}\right] \quad (30)$$

$$\alpha_{R,1,j} = H\left[\frac{\delta F_{C,NPP,j}}{\delta C_{R,1,j}} - \frac{\delta F_{C,NPP,j}}{\delta C_{L,j}}\right] H\left[\frac{\delta F_{C,NPP,j}}{\delta C_{R,1,j}} - \frac{\delta F_{C,NPP,j}}{\delta C_{R,2,j}}\right] \quad (31)$$

$$\alpha_{R,2,j} = H\left[\frac{\delta F_{C,NPP,j}}{\delta C_{R,2,j}} - \frac{\delta F_{C,NPP,j}}{\delta C_{L,j}}\right] H\left[\frac{\delta F_{C,NPP,j}}{\delta C_{R,2,j}} - \frac{\delta F_{C,NPP,j}}{\delta C_{R,1,j}}\right] \quad (32)$$

Where H is the Heaviside Step Function, the value of which is zero for a negative argument and one for a positive argument. Partial derivatives in Eqs. (30)–(32) are readily evaluated from analytically differentiating $F_{C,NPP,j}$ with respect to each plant carbon pool.

For trees, the total allocation to leaves and wood is partitioned, such that a target ratio of leaf area to sapwood area, $k_{LA:SA}$ is maintained:

$$\frac{(C_{L,w} + \alpha_{L,w} F_{C,Growth,w} - k_{L,w} C_{L,w}) A_{SL,w}}{A_{sapwood}} \leq k_{LA:SA} \quad (33)$$

where $A_{SL,w}$ is the specific leaf area for woody vegetation (see Eq. 38 below).

2.2.7 Vegetation cover

The vegetation cover fraction or green-leaf cover n (dimensionless, between 0 and 1) is assumed equal to the fraction of absorbed photosynthetically active radiation (FAPAR) and related to leaf area index L by

$$v_{tree} = 1 - \exp(-c_{Ext} K_{clump} \Lambda_w) \quad (34)$$

and

$$v_g = (1 - v_g)(1 - \exp(-c_{Ext} \Lambda_g)) \quad (35)$$

where c_{Ext} is the exponential light extinction coefficient in the canopy (assumed here the same for trees and grass), and K_{clump} is a crown clumping factor related to crown projected cover A_c by (Haverd et al., 2012),

$$K_{Clump} = \min[A_c(1.0 - \exp(-c_{Ext} \Lambda_w / A_c))/(c_{Ext} \Lambda_w), 1.0] \quad (36)$$

as computed within the POP module.

Leaf area index is related to the leaf carbon pool and specific leaf area A_{SL} [$cm^2\,g(DW)^{-1}$] by:

$$\Lambda_j = 0.0024 \frac{g(DW)\,cm^{-2}}{mol\,C\,m^{-2}} A_{SL,j} C_{L,j} \quad (37)$$

For woody vegetation, specific leaf area is known to increase with mean annual precipitation (P, $mm\,yr^{-1}$) along the NATT as (Schulze et al., 1998):

$$A_{SL,w} = 2.0 + 0.025P \quad (38)$$

2.3 Woody biomass turnover and tree demography feed-backs on carbon uptake

Woody biomass turnover due to resource-limitation mortality and disturbance mortality (including fire mortality) is computed by coupling HAVANA to the POP module for tree demography and landscape heterogeneity mediated by disturbance. POP has been fully described elsewhere (Haverd et al., 2014), except for updates used in this work, relating to the feed-backs of structure on function, which are documented in Appendix A.

3 Study site and observational data

The North Australian Tropical Transect is a 1000 km transect (Hutley et al., 2011), with a systematic decline in mean annual rainfall (Grant et al., 2008; Jones et al., 2009) with distance ($\sim 1\,mm\,km^{-1}$) from the northern coast of the Northern Territory, Australia. As in (Haverd et al., 2013b), we represent the gradients in rainfall (Fig. 2ii) and fire regime (Fig. 2iii) of the NATT transect by selecting 1000 random 0.05° × 0.05° grid-cells from an area bounded by (19.95, 11.4° S, 130.0, 134.5° E) (Fig. 2i). The NATT is characterized by largely intact savanna vegetation. In the north of the region (mean annual precipitation > 600 mm), the dominant vegetation is tropical savanna (overstorey of evergreen *Eucalyptus* and *Corymbia* tree species, and an understorey dominated by C4 grasses), while Acacia wood-lands, shrublands and hummock grasslands become increasingly prominent at the southern, semi-arid extreme (Hutley et al., 2011). The vegetation is subjected to fire regularly (once every 2 to 7 yr, Fig. 2ii, data derived from Craig et al., 2002), which allows curing of C4 grasses and litter. The fraction of early

dry-season (pre-August) fires follows a similar latitudinal pattern to the fire frequency, which is an effect of fire management. Fire timing is a predictor of fire intensity, with late-season fires generally being significantly more intense as fuels accumulate and cure and weather becomes more extreme (Williams et al., 1998).

3.1 Driving data

HAVANA was forced using gridded meteorological data and soil properties at 0.05° spatial resolution, which are described fully in Haverd et al. (2013a). Briefly, meteorological data comprise daily gridded rainfall, temperature, and solar irradiance for the period 1900–2013, current at March 2014, from the Bureau of Meteorology's Australian Water Availability Project data set (BoM AWAP) (Grant et al., 2008; Jones et al., 2009), with temporal gap-filling using climatologies from the same dataset. Soil information is taken from the McKenzie and Hook (1992) and McKenzie et al. (2000) interpretations of the 725 principal profile forms (soil types) mapped in the Digital Atlas of Australian Soils (Northcote et al., 1960, 1975).

3.2 Data for model calibration and validation

3.2.1 Calibration data

Monthly Estimates of GPP and ET from five flux tower sites (Table 2 and located in Fig. 2i) were obtained from eddy covariance datasets that were quality assured and quality controlled using the OzFlux standard processing protocol OzFluxQCv2.8.5 (Eamus et al., 2013), (Isaac et al., in preparation for this special issue). Gaps in missing data were filled, and GPP was resolved from net ecosystem exchange (NEE) using a new processing package called DINGO (Dynamic INtegrated Gap filling and partitioning for OzFlux).

DINGO applies a linear interpolation to gaps of less than two hours, and uses the following methods for gaps longer than two hours. For temperature, humidity, pressure,

precipitation and wind speed, DINGO searches for the 10 closest Australian Bureau of Meteorology (BoM) monitoring sites from a localised database and gap fills using data from the site for which correlation with site data is the highest. Gaps in incoming solar radiation gaps are filled using solar exposure data, derived by the BoM from satellite imagery, while reflected solar radiation is filled using the MODIS albedo product. Soil moisture and temperature gaps are filled from half-hourly outputs from a biogeochemical land surface model, constrained by observations of land–atmosphere fluxes, biomass, streamflow and remotely sensed vegetation cover (Haverd et al., 2013a). A feed-forward artificial neural network (ANN), described in Beringer et al. (2007), is used to gap fill NEE and sensible, latent, and soil heat fluxes.

DINGO estimates GPP as NEE minus ecosystem respiration (R_e), with R_e estimated as follows. During the night, CO_2 fluxes are assumed to equal R_e, as no photosynthesis occurs. It is also assumed that NEE, being biologically determined, is independent of atmospheric turbulence and remains constant above a friction velocity (u*) threshold (Goulden et al., 1996), also assuming that stored CO_2 is drained completely from beneath the canopy before re-initiation of turbulence (Aubinet, 2008) This last assumption is likely to be violated at the southern-most Alice Springs site (Cleverly et al., 2013). Based on these assumptions, we used a u* threshold for selecting nights of adequate ventilation to determine the respiration component of carbon flux. The u* threshold applied is based on Reichstein et al. (2005), where the u* filtering dataset is split into six equal sample size temperature classes, and into 20 u* classes within each temperature class. When the u* value falls below the threshold, DINGO removes the value of NEE during that half-hour and the subsequent half-hour. The maximum u* threshold and gap filled soil moisture, soil temperature, air temperature and normalised difference vegetation index (NDVI) variables are inputs to an ANN for calculating R_e.

A monthly time series of vegetation fractional cover (fPAR) for January 1982 to December 2013 was derived from the third generation (NDVI3g) of the GIMMS NDVI time series (Tucker et al., 2005; Zhu et al., 2013). A monthly maximum composite was created from the original 15 d series, and the data were resampled from the original

0.0833° resolution (8 km) to 0.05° (5 km). NDVI values from 0.1 (bare ground) to 0.75 (full cover) were linearly rescaled between 0 and 1 to represent vegetation fractional cover. For calibration, we used 2000–2013 data at the locations of the flux sites (Table 1).

3.2.2 Validation data

For model evaluation, we used predictive empirical models describing the decline of basal area and projected foliage cover with rainfall, developed by Williams et al. (1996) from a data-set of ~ 1000 quadrats (each 20 m × 20 m) lying north of 18° S within the Northern Territory. We also utilized observations reported by Sea et al. (2011) of dry-season (September 2008) tree leaf area index (LAI) based both on digital hemispheric photography (DHP) and the MODIS Collection 5 (MODC5) remote-sensing LAI product. Additionally we used monthly fPAR (as described in *Calibration Data* above) along the entire rainfall gradient.

4 Model–data fusion

We calibrated HAVANA parameters by optimisation against monthly observations of ET, GPP and fPAR, subject to prior constraints. The search algorithm was the Levenberg–Marquardt method implemented in the PEST software package (Doherty, 2004). The cost function to be minimised was the weighted sum of squared residuals, $\Phi = \sum_j w_i^2 r_i^2$, where the residual r_i can be either the residual between a model prediction and corresponding observation, or the residual between prior and posterior variables. Relative observation weights (w_i) were set such that each observation data type and each prior constraint contributed equally to the prior cost function.

Prior constraints consisted of estimates of leaf and fine-root carbon pools at Howard Springs. We assume prior estimates of time-averaged leaf carbon to be 50 and 100 g C m^{-2} for grassy and woody vegetation respectively, and a ratio of time-averaged

fine root mass to leaf mass of 2. Leaf carbon estimates are based on Chen et al. (2003). The ratio of fine root to leaf mass is a very rough estimate, as estimates of peak fine root mass in Northern Australian tropical savannas are divergent: 1800 g C m^{-2} (Janos et al., 2008); 50 g C m^{-2}; 140 g C m^{-2} (claimed to be a factor of 10 too low by Janos et al., 2008).

5 Results

5.1 Calibration

We assessed the calibrated HAVANA predictions of monthly fluxes of ET and GPP, and monthly mean remotely-sensed fPAR. Time series of the three modelled variables for each flux site are shown in Fig. 3 as coloured patches, with colour coding to represent the flux-partitioning between transpiration from upper and lower soil and soil evaporation (ET) and between tree and grass components (fPAR and GPP). The observed quantities are also shown along with a benchmark, being a state-of-the-art biogeochemical land surface model (CABLE, as implemented in BIOS2, Haverd et al., 2013a), forced using LAI derived from the GIMMS-3g fPAR product (Zhu et al., 2013), and calibrated here against GPP and ET from the five flux sites. ET, fPAR and GPP determined from HAVANA-POP increasingly matched observations toward the northern end of the NATT, where a more predictable seasonal cycle was observed than at the southernmost semi-arid site (Fig. 4). Even without being supplied external vegetation cover information, our new HAVANA model performed equally well or better than the benchmark (BIOS2) for monthly GPP and ET, as illustrated by slightly larger R^2 values and slightly smaller RMSE scores (Fig. 4). There was a tendency in HAVANA and BIOS2 to under-predict ET (slope > 1), whereas the modelled range in GPP closely matched the observed range (Fig. 4). While ET, and to a lesser extent GPP, was under-predicted by BIOS2 at Howard Springs, the bias was not apparent in the HAVANA results (Fig. 4). Both models over-predict the small values of ET and GPP at

the Alice Springs site (Fig. 4). HAVANA soil evaporation is a small proportion of ET at all sites.

5.2 Evaluation

We evaluated the performance of HAVANA-POP along the entire rainfall gradient (Fig. 5). Each model point represents a spatial average across ~ 65 points lying within a latitude bin of width 0.57°, with error bars representing one standard deviation. The model replicates observed variations with rainfall of GPP, foliage projective cover, tree basal area and dry season tree LAI along the transect. Modelled tree foliage projective cover is higher than the observation-based estimates by about 0.06. This likely reflects a bias between the observation-based estimates, and the satellite-based fPAR that was used for calibration.

5.3 HAVANA dynamics along the NATT

Figure 6a and b illustrates the dynamics of key HAVANA variables from north (top row) to south (bottom row) along the NATT. Soil moisture (Fig. 6a(i)) shows strong seasonality in the top layer, which is smoothed out in the lower layer, resulting in respective seasonal and persistent transpiration (root water extraction) from the two layers (Fig. 6a(ii)). This leads to woody vegetation cover persisting throughout the year (Fig. 6a(iii–iv)) and only small seasonal fluctuations in associated GPP (Fig. 6a(v)), compared with grassy vegetation cover, which is completely absent by the late dry season. The decline in fPAR southward along the NATT accords well with satellite obervations (Fig. 6a(iv)), as does the interannual variability which is largely absent at the northern end of the NATT, and clearly evident below 970 mm MAP.

Grassy vegetation is characterised by significant temporal shifts in NPP and growth, leading to large changes in the NSC store (Fig. 6b(i)). This ability for growth to draw on NSC reserves is critical for rapid production of resource uptake surfaces (leaves and roots) at the beginning of the wet season (Fig. 6b(iii)). The change in storage flux (relative to NPP) increases down the transect as both woody and grassy vegetation become more reliant on the NSC pool for growth in times of stress (Fig. 6b(i, ii)). For grass, root carbon increases with aridity relative to leaf carbon. This is less evident for woody vegetation, because leaf carbon in woody vegetation is also influenced by a gradient in specific leaf area (Eq. 38). Allocation patterns for grass (Fig. 6b(v)) show an increasing fine root component as aridity increases down the transect, with temporal dynamics dictated by whether fine roots or leaves are limiting NPP (Eqs. 30–31). (These are monthly-averaged C-allocation coefficients, which don't necessarily sum to one because allocation coefficients are zero when growth is zero.) For trees (Fig. 6b(vi)), allocation to surface roots occurs in the early wet season, when soil moisture in the upper layer exceeds that in the lower layer. Thus tree and grass roots compete in the surface layer. When soil moisture is plentiful (e.g. 2011), root growth is small and the remainder is partitioned between stems and leaves (Fig. 6b(vi)). Leaf carbon is constrained by sapwood area (Eq. 33), leading to periods of high allocation to stems in wet periods.

6 Discussion

There is ongoing debate about the mechanisms governing tree and grass cover and maintaining the stability of savanna ecosystems relative to grassland or closed woody ecosystems (Bond, 2008; Torello-Raventos et al., 2013). While it is widely acknowledged that both resource limitation (especially water) and disturbance (fire and grazing) may control tree cover, their roles differ along environmental gradients and between continents (Africa, Australia, and South America), to the extent that Lehmann et al. (2014) claimed that "a single model cannot adequately represent savanna woody biomass across these regions". Sankaran et al. (2005) found woody carrying capacity in African savannas to be limited by rainfall, but that savannas were typically held below woody carrying capacity by fire or grazing. Supporting the influential role of disturbance, Bond et al. (2005) used a dynamic vegetation model to infer that fire suppres-

sion has the potential to convert vast areas of C4 grassland and savannas to forests, roughly doubling the global area covered by forest. Sea and Hanan (2012) highlight the importance of self-thinning of smaller trees as they compete with grass for resources, in contrast to the Walter hypothesis (Ward et al., 2013) that tree-grass co-existence is made possible by separation of the rooting niche. While root partitioning is important in controlling relative performance of trees and grasses (e.g. Kulmatiski and Beard, 2013), there is good evidence that long-term stand dynamics are modulated by life-history disturbance interactions on demography (Higgins et al., 2000).

In Australian savannas (in contrast to other continents), Bond (2008) noted a roughly linear relationship between mean annual precipitation and tree cover, indicative of a stronger limitation by water availability and less impact from fire given the remarkable fire tolerance of the dominant woody genera of Australian savanna, *Eucalyptus* and *Corymbia* (Lawes et al., 2011). Murphy et al. (2015) suggested that fire impacts controlling *Eucalyptus* and *Corymbia* woody cover have been exaggerated in north Australian savanna, with intraspecific competition for limited water and nutrient resources a far stronger driver of cover. This finding is supported by the high proportion of biomass loss attributable to resource-limitation in HAVANA-POP. According to our model, of the total biomass lost to mortality, 68 % is attributable to resource-limitation at the wet northern end of the NATT, increasing to 84 % at the arid southern end. The remaining minority of biomass turnover is attributable to disturbance loss, largely from fire.

7 Future prospects

The principles encoded in HAVANA-POP have been demonstrated to suffice as a "single-model" to account for savanna tree cover for the case of Australia. However the model in its current form has limitations, warranting further development for use in carbon-water-nutrient cycle modelling. For example: (i) nutrient resources are not accounted for, (ii) fire frequency is prescribed, (iii) leaves have a fixed turnover rate, which may explain e.g. the lack of modelled seasonality in tree vegetation cover (Fig. 6a(iv)),

known from observations to have an amplitude of about 30 % at the northern end of the transect (Chen et al., 2003), (iv) soil evaporation (Fig. 4i) is low compared with limited observations (e.g. Hutley et al., 2000, observed soil evaporation fluxes that accounted for 50 % of total evapotranspiration during the wet season at Howard Springs).

To overcome the above limitations, and to test the HAVANA principles of coupled allocation-phenology describing savannas globally, future work will entail implementation these principles within a full biogeochemical land-surface model, coupled to the POP module for tree demography and landscape heterogeneity (e.g. CABLE-POP (Haverd et al., 2014)). In particular we propose implementing formulations developed here for growth (Eq. 19), NSC dynamics via coupling of growth and NPP (Eq. 21) and dynamic C allocation to maximise long-term NPP (Eqs. 30–32), while maintaining sufficient sapwood cross-sectional area to support leaf transpiration (Eq. 33). Such an implementation would require the following of the (modified) biogeochemical model: (i) root-water extraction dependence on root carbon, (ii) association of root carbon with vertical structure of soil moisture stores, (iii) partial derivatives of NPP (and hence GPP) with respect to plant carbon stores. Since GPP in the biogeochemical model may not be analytically differentiable, we suggest running the HAVANA GPP model (Eq. 23) in parallel with the full GPP model at daily time scale and with key parameters (water-use and light-use efficiencies) supplied by the full model at each daily time-step.

8 Conclusion

We have shown that HAVANA-POP predicts tree/grass partitioning along a wide rainfall gradient within a biozone of the Australian savanna belt. The model behaviour emerges from complex feed-backs (Fig. 1) between the plant physiology and vegetation dynamics, mediated by shifting above- vs. below-ground resources, and not from imposed hypotheses about the controls on tree/grass co-existence.

Appendix A: Updates to the POP module

POP simulates woody ecosystem stand dynamics, demography and disturbance-mediated heterogeneity. In previous work, POP has been coupled to the CABLE land surface scheme (Wang et al., 2011) and demonstrated to successfully replicate both the effects of rainfall and fire disturbance gradients on vegetation structure along the NATT (Haverd et al., 2013b), and leaf-stem allometric relationships derived from global forest data (Haverd et al., 2014).

A1 POP coupling

In the above-mentioned applications, the CABLE-POP coupling consisted of just two exchanges: (i) stem NPP passed from the host LSM to POP, (ii) woody biomass turnover returned from POP to the host LSM. In contrast, in the current work, the HAVANA-POP coupling also includes the return of sapwood area and sapwood volume to HAVANA, where these variables respectively influence C-allocation to leaves (Eq. 33) and autotrophic respiration (Eq. 28). Further, in previous applications of POP, LAI was exogenous, being imposed using remote-sensing. In contrast, in the HAVANA-POP set-up, LAI is endogenous, being computed from leaf carbon (Eq. 37). Figure A1 illustrates the HAVANA-POP coupling and key inputs and outputs.

A2 POP Biomass partitioning amongst patches and cohorts

Stem biomass increment for each patch ΔC ($\mathrm{kg\,C\,m^{-2}}$), is assumed equal to the grid-scale value, accumulated over the POP model time step Dt (yr).

In the original model, it was assumed that individuals capture resources in a varying proportion to their size, following a power relationship to biomass with an exponent (s). On this basis, annual stem biomass increment was partitioned among cohorts in proportion to the population-weighted current biomass of individuals within each

cohort:

$$\frac{\Delta C_y}{\Delta t} = \frac{(C_y/N_y)^s N_y}{\sum (C_i/N_i)^s N_i} \frac{\Delta C}{\Delta t} \tag{A1}$$

where C_y is the stem biomass summed across individuals of cohort N_y.

In the current work, gross primary production and autotrophic respiration are each passed from the host model to POP, and each is partitioned amongst patches and cohorts. Net resource uptake for each patch and cohort is evaluated as its gross primary production minus autotrophic respiration.

Gross resource uptake ΔC_g is partitioned amongst cohorts and patches in proportion to light interception, evaluated from vertical profiles of gap probabilities. These require the maximum leaf area $\mathrm{LAI_{max}}$, inherited from the host model to be partitioned amongst patches and cohorts in proportion to sapwood area in the yth cohort and pth patch $A_{\mathrm{s},y,p}$:

$$\mathrm{LAI}_{\mathrm{max},y,p} = N_{y,p} A_{\mathrm{s},y,p} \frac{\sum_{x=1}^{y_{\max}} N_{x,p} A_{\mathrm{s},x,p}}{\sum_{j=1}^{n_p} w_j \left(\sum_{x=1}^{y_{\max}} N_{x,j} A_{\mathrm{s},x,j} \right)} \mathrm{LAI_{max}} \tag{A2}$$

Autotrophic respiration is also partitioned amongst cohorts and patches, with leaf and root carbon pools partitioned in proportion to LAI.

Stem biomass is the sum of sapwood $C_{\mathrm{s},y,p}$ and heartwood components $C_{\mathrm{h},y,p}$, with sapwood converted to heartwood at a rate $k_\mathrm{s} = 0.05\,\mathrm{yr^{-1}}$:

$$\frac{\Delta C_{\mathrm{s},y,p}}{\Delta t} = \frac{\Delta C_{y,p}}{\Delta t} - k_\mathrm{s} C_{\mathrm{s},y,p} \tag{A3}$$

$$\frac{\Delta C_{\mathrm{h},y,p}}{\Delta t} = k_\mathrm{s} C_{\mathrm{s},y,p} \tag{A4}$$

The sapwood area is related to sapwood biomass and tree dimensions by:

$$A_{s,y,p} = \frac{\pi D_{y,p}^2}{4} - \frac{C_{y,p} - C_{s,y,p}}{H_{y,p} N_{y,p} \rho_w} \quad \text{(A5)}$$

Sapwood area is returned to the host model, where it constrains the relative C-allocation to leaves and wood (Eq. 33).

Acknowledgements. The contributions of VH and PRB were made possible by the support of the Australian Science Change Program. BS acknowledges funding as an OCE Distinguished Visiting Scientist to the CSIRO Oceans & Atmosphere Flagship, Canberra.

We are grateful to Ranga Myneni and Jian Bi for the supply of GIMMS NDVI3g updated to 2013, and to Randall Donohue for processing of these data for this study. This study is a contribution to the strategic research areas BECC and MERGE.

References

Ahlström, A., Raupach, M. R., Schurgers, G., Smith, B., Arneth, A., Jung, M., Reichstein, M., Canadell, J. G., Friedlingstein, P., Jain, A. K., Kato, E., Poulter, B., Sitch, S., Stocker, B. D., Viovy, N., Wang, Y. P., Wiltshire, A., Zaehle, S., and Zeng, N.: The dominant role of semi-arid ecosystems in the trend and variability of the land CO_2 sink, Science, 348, 895–899, 2015.

Aubinet, M.: Eddy covariance CO_2 flux measurements in nocturnal conditions: an analysis of the problem, Ecol. Appl., 18, 1368–1378, 2008.

Baudena, M., Dekker, S. C., van Bodegom, P. M., Cuesta, B., Higgins, S. I., Lehsten, V., Reick, C. H., Rietkerk, M., Scheiter, S., Yin, Z., Zavala, M. A., and Brovkin, V.: Forests, savannas, and grasslands: bridging the knowledge gap between ecology and Dynamic Global Vegetation Models, Biogeosciences, 12, 1833–1848, doi:10.5194/bg-12-1833-2015, 2015.

Beringer, J., Hutley, L., Tapper, N., Coutts, A., Kerley, A., and O'grady, A.: Fire impacts on surface heat, moisture and carbon fluxes from a tropical savanna in northern Australia, Int. J. Wildland Fire, 12, 333–340, 2003.

Beringer, J., Hutley, L. B., Tapper, N. J., and Cernusak, L. A.: Savanna fires and their impact on net ecosystem productivity in North Australia, Glob. Change Biol., 13, 990–1004, 2007.

Beringer, J., Hutley, L. B., Hacker, J. M., Neininger, B., and U, K. T. P.: Patterns and processes of carbon, water and energy cycles across northern Australian landscapes: from point to region, Agr. Forest Meteorol., 151, 1409–1416, 2011.

Bond, W. J.: What limits trees in C4 grasslands and savannas?, Annu. Rev. Ecol. Evol. S., 39, 641–659, 2008.

Bond, W. J., Woodward, F. I., and Midgley, G. F.: The global distribution of ecosystems in a world without fire, New Phytol., 165, 525–538, 2005.

Chen, X., Hutley, L. B., and Eamus, D.: Carbon balance of a tropical savanna of northern Australia, Oecologia, 137, 405–416, 2003.

Choler, P., Sea, W., Briggs, P., Raupach, M., and Leuning, R.: A simple ecohydrological model captures essentials of seasonal leaf dynamics in semi-arid tropical grasslands, Biogeosciences, 7, 907–920, doi:10.5194/bg-7-907-2010, 2010.

Cleverly, J., Boulain, N., Villalobos-Vega, R., Grant, N., Faux, R., Wood, C., Cook, P. G., Yu, Q., Leigh, A., and Eamus, D.: Dynamics of component carbon fluxes in a semi-aridAcaciawoodland, central Australia, J. Geophys. Res.-Biogeo., 118, 1168–1185, doi:10.1002/jgrg.20101, 2013.

Craig, R., Heath, B., Raisbeck-Brown, N., Steber, M., Marsden, J., and Smith, R.: The Distribution, Extent and Seasonality of Large Fires in Australia, April 1998–March 2000, as Mapped from NOAA–AVHRR Imagery, Department of the Environment and Heritage, Canberra, 2002.

Doherty, J.: PEST, Watermark Numerical Computing, Townesville, 2004.

Donohue, R. J., McVicar, T. R., and Roderick, M. L.: Climate-related trends in Australian vegetation cover as inferred from satellite observations, 1981–2006, Glob. Change Biol., 15, 1025–1039, 2009.

Eamus, D., Cleverly, J., Boulain, N., Grant, N., Faux, R., and Villalobos-Vega, R.: Carbon and water fluxes in an arid-zone Acacia savanna woodland: an analyses of seasonal patterns and responses to rainfall events, Agr. Forest Meteorol., 182–183, 225–238, 2013.

Franklin, O., Johansson, J., Dewar, R. C., Dieckmann, U., McMurtrie, R. E., Brannstrom, A., and Dybzinski, R.: Modeling carbon allocation in trees: a search for principles, Tree Physiol., 32, 648–666, 2012.

Goulden, M. L., Munger, J. W., Song-Miao, F., Daube, B. C., and Wofsy, S. C.: Measurements of carbon sequestration by long-term eddy covariance: methods and a critical evaluation of accuracy, Glob. Change Biol., 2, 169–182, 1996.

Grant, I., Jones, D., Wang, W., Fawcett, R., and Barratt, D.: Meteorological and remotely sensed datasets for hydrological modelling: a contribution to the Australian Water Availability Project, Melbourne, January 9–11, 2008.

Haverd, V., Raupach, M. R., Briggs, P. R., Canadell, J. G., Isaac, P., Pickett-Heaps, C., Roxburgh, S. H., van Gorsel, E., Viscarra Rossel, R. A., and Wang, Z.: Multiple observation types reduce uncertainty in Australia's terrestrial carbon and water cycles, Biogeosciences, 10, 2011–2040, doi:10.5194/bg-10-2011-2013, 2013a.

Haverd, V., Smith, B., Cook, G. D., Briggs, P. R., Nieradzik, L., Roxburgh, S. H., Liedloff, A., Meyer, C. P., and Canadell, J. G.: A stand-alone tree demography and landscape structure module for Earth system models, Geophys. Res. Lett., 40, 5234–5239, 2013b.

Haverd, V., Smith, B., Nieradzik, L. P., and Briggs, P. R.: A stand-alone tree demography and landscape structure module for Earth system models: integration with inventory data from temperate and boreal forests, Biogeosciences, 11, 4039–4055, doi:10.5194/bg-11-4039-2014, 2014.

Hutley, L. B., O'Grady, A. P., and Eamus, D.: Evapotranspiration from Eucalypt open-forest savanna of Northern Australia, Funct. Ecol., 14, 183–194, 2000.

Hutley, L. B., Beringer, J., Isaac, P. R., Hacker, J. M., and Cernusak, L. A.: A sub-continental scale living laboratory: spatial patterns of savanna vegetation over a rainfall gradient in northern Australia, Agr. Forest Meteorol., 151, 1417–1428, 2011.

Janos, D. P., Scott, J., and Bowman, D. M. J. S.: Temporal and spatial variation of fine roots in a northern Australian Eucalyptus tetrodonta savanna, J. Trop. Ecol., 24, 177–188, 2008.

Jones, D. A., Wang, W., and Fawcett, R.: High-quality spatial climate data-sets for Australia, Austr. Meteorol. Oceanogr. J., 58, 233–248, 2009.

Kulmatiski, A. and Beard, K. H.: Woody plant encroachment facilitated by increased precipitation intensity, Nature Climate Change, 3, 833–837, 2013.

Lawes, M., Richards, A., Dathe, J., and Midgley, J.: Bark thickness determines fire resistance of selected tree species from fire-prone tropical savanna in north Australia, Plant Ecol., 212, 2057–2069, 2011.

Lehmann, C. E., Anderson, T. M., Sankaran, M., Higgins, S. I., Archibald, S., Hoffmann, W. A., Hanan, N. P., Williams, R. J., Fensham, R. J., and Felfili, J.: Savanna vegetation–fire–climate relationships differ among continents, Science, 343, 548–552, 2014.

Lehmann, C. E. R., Prior, L. D., and Bowman, D. M. J. S.: Decadal dynamics of tree cover in an Australian tropical savanna, Austral. Ecol., 34, 601–612, 2009.

Liu, Y. Y., van Dijk, A. I. J. M., de Jeu, R. A. M., Canadell, J. G., McCabe, M. F., Evans, J. P., and Wang, G.: Recent reversal in loss of global terrestrial biomass, Nature Climate Change, 5, 470–474, 2015.

Lloyd, J. and Taylor, J. A.: On the temperature dependence of soil respiration, Funct. Ecol., 8, 315–323, 1994.

Ma, X., Huete, A., Yu, Q., Coupe, N. R., Davies, K., Broich, M., Ratana, P., Beringer, J., Hutley, L. B., Cleverly, J., Boulain, N., and Eamus, D.: Spatial patterns and temporal dynamics in savanna vegetation phenology across the North Australian Tropical Transect, Remote Sens. Environ., 139, 97–115, 2013.

McDowell, N., Barnard, H., Bond, B., Hinckley, T., Hubbard, R., Ishii, H., Kostner, B., Magnani, F., Marshall, J., Meinzer, F., Phillips, N., Ryan, M., and Whitehead, D.: The relationship between tree height and leaf area: sapwood area ratio, Oecologia, 132, 12–20, 2002.

McKenzie, N. J. and Hook, J.: Interpretation of the Atlas of Australian Soils, technical report 94/1992, CSIRO Division of Soils, Canberra, 1992.

McKenzie, N. J., Jacquier, D. W., Ashton, L. J., and Creswell, H. P.: Estimation of Soil Properties Using the Atlas of Australian Soils, Canberra, 24 pp., 2000.

Murphy, B. P., Liedloff, A. C., and Cook, G. D.: Does fire limit tree biomass in Australian savannas?, Int. J. Wildland Fire, 24, 1–13, 2015.

Northcote, K. H., Beckmann, G. G., Bettenay, E., Churchward, H. M., Van Dijk, D. C., Dimmock, G. M., Hubble, G. D., Isbell, R. F., McArthur, W. M., Murtha, G. G., Nicolls, K. D., Paton, T. R., Thompson, C. H., Webb, A. A., and Wright, M. J.: Atlas of Australian Soils, Sheets 1 to 10, with Explanatory Data, CSIRO Australia and Melbourne University Press, Melbourne, 1960.

Northcote, K. H., Hubble, G. D., Isbell, R. F., Thompson, C. H., and Bettenay, E.: A Description of Australian Soils, CSIRO Australia, 1975.

Poulter, B., Frank, D., Ciais, P., Myneni, R. B., Andela, N., Bi, J., Broquet, G., Canadell, J. G., Chevallier, F., Liu, Y. Y., Running, S. W., Sitch, S., and van der Werf, G. R.: Contribution of semi-arid ecosystems to interannual variability of the global carbon cycle, Nature, 509, 600–603, 2014.

Priestley, C. H. B. and Taylor, R. J.: On the assessment of surface heat flux and evaporation using large-scale parameters, Mon. Weather Rev., 100, 81–92, 1972.

Raupach, M. R.: Influences of local feedbacks on land–air exchanges of energy and carbon, Glob. Change Biol., 4, 477–494, 1998.

Raupach, M. R.: Equilibrium evaporation and the convective boundary layer, Bound.-Lay. Meteorol., 96, 107–142, 2000.
Raupach, M. R.: Combination theory and equilibrium evaporation, Q. J. Roy. Meteor. Soc., 127, 1149–1181, 2001.
Raupach, M. R.: Dynamics and optimality in coupled terrestrial energy, water, carbon and nutrient cycles, in: Predictions in Ungauged Basins: International Perspectives on the State of the Art and Pathways Forward 2005, edited by: Franks, S. W. S., Takeuchi, M., Tachikawa, K. Y., 223–238, 2005.
Raupach., M. R. R., Briggs, P. R., Haverd, V., King, E. A., Paget, M., and Trudinger, C. M.: Australian Water Availability Project (AWAP): CSIRO Marine and Atmospheric Research Component: Final Report for Phase 3, Canberra, 67 pp., 2009.
Reichstein, M., Falge, E., Baldocchi, D., Papale, D., Aubinet, M., Berbigier, P., Bernhofer, C., Buchmann, N., Gilmanov, T., Granier, A., Grünwald, T., Havránková, K., Ilvesniemi, H., Janous, D., Knohl, A., Laurila, T., Lohila, A., Loustau, D., Matteucci, G., Meyers, T., Miglietta, F., Ourcival, J. M., Pumpanen, J., Rambal, S., Rotenberg, E., Sanz, M., Tenhunen, J., Seufert, G., Vaccari, F., Vesala, T., Yakir, D., and Valentini, R.: On the separation of net ecosystem exchange into assimilation and ecosystem respiration: review and improved algorithm, Glob. Change Biol., 11, 1424–1439, 2005.
Ryan, M. G.: Effects of climate change on plant respiration, Ecol. Appl., 1, 157–167, 1991.
Sankaran, M., Hanan, N. P., Scholes, R. J., Ratnam, J., Augustine, D. J., Cade, B. S., Gignoux, J., Higgins, S. I., Le Roux, X., and Ludwig, F.: Determinants of woody cover in African savannas, Nature, 438, 846–849, 2005.
Scheiter, S. and Higgins, S. I.: Impacts of climate change on the vegetation of Africa: an adaptive dynamic vegetation modelling approach, Glob. Change Biol., 15, 2224–2246, 2009.
Scholes, R. J. and Walker, B. H.: An African Savanna: Synthesis of the Nylsvley Study, Cambridge University Press, 2004.
Schulze, E.-D., Williams, R., Farquhar, G., Schulze, W., Langridge, J., Miller, J., and Walker, B. H.: Carbon and nitrogen isotope discrimination and nitrogen nutrition of trees along a rainfall gradient in northern Australia, Funct. Plant Biol., 25, 413–425, 1998.
Schymanski, S. J., Sivapalan, M., Roderick, M. L., Hutley, L. B., and Beringer, J.: An optimality-based model of the dynamic feedbacks between natural vegetation and the water balance, Water Resour. Res., 45, W01412, doi:10.1029/2008WR006841, 2009.

Sea, W. B., Choler, P., Beringer, J., Weinmann, R. A., Hutley, L. B., and Leuning, R.: Documenting improvement in leaf area index estimates from MODIS using hemispherical photos for Australian savannas, Agr. Forest Meteorol., 151, 1453–1461, 2011.
Sea, W. B. and Hanan, N. P.: Self-thinning and tree competition in savannas, Biotropica, 44, 189–196, 2012.
Shinozaki, K., Yoda, K., Hozumi, K., and Kira, T.: A quantitative analysis of plant form – the Pipe Model Theory I. Basic analyses, Japanese J. Ecol., 14, 97–105, 1964.
Singh, K. P. and Misra, G.: Water-use efficiency of one C3 and two C4 grasses in response to varying soil moisture and herbage-removal levels in a seasonally dry tropical region, Plant Soil, 88, 171–180, 1985.
Sitch, S., Smith, B., Prentice, I. C., Arneth, A., Bondeau, A., Cramer, W., Kaplan, J., Levis, S., Lucht, W., and Sykes, M. T.: Evaluation of ecosystem dynamics, plant geography and terrestrial carbon cycling in the LPJ dynamic global vegetation model, Glob. Change Biol., 9, 161–185, 2003.
Sprugel, D. G., Ryan, M. G., Brooks, J., Vogt, K., and Martin, T. A.: Respiration from the organ level to the stand, Resource Physiology of Conifers, 8, 255–299, 1995.
Swinbank, W. C.: Long-wave radiation from clear skies, Q. J. Roy. Meteor. Soc., 89, 339–348, 1963.
Torello-Raventos, M., Feldpausch, T. R., Veenendaal, E., Schrodt, F., Saiz, G., Domingues, T. F., Djagbletey, G., Ford, A., Kemp, J., and Marimon, B. S.: On the delineation of tropical vegetation types with an emphasis on forest/savanna transitions, Plant Ecol. Div., 6, 101–137, 2013.
Tucker, C. J., Pinzon, J. E., Brown, M. E., Slayback, D. A., Pak, E. W., Mahoney, R., Vermote, E. F., and El Saleous, N.: An extended AVHRR 8 km NDVI dataset compatible with MODIS and SPOT vegetation NDVI data, Int. J. Remote Sens., 26, 4485–4498, 2005.
Vogt, K., Vogt, D., Palmiotto, P., Boon, P., O'Hara, J., and Asbjornsen, H.: Review of root dynamics in forest ecosystems grouped by climate, climatic forest type and species, Plant Soil, 187, 159–219, 1995.
Von Caemmerer, S.: Biochemical Models of Leaf Photosynthesis, Csiro publishing, 2000.
Wang, Y. P., Kowalczyk, E., Leuning, R., Abramowitz, G., Raupach, M. R., Pak, B., van Gorsel, E., and Luhar, A.: Diagnosing errors in a land surface model (CABLE) in the time and frequency domains, J. Geophys. Res.-Biogeo., 116, G01034, doi:10.1029/2010JG001385, 2011.

Ward, D., Wiegand, K., and Getzin, S.: Walter's two-layer hypothesis revisited: back to the roots!, Oecologia, 172, 617–630, 2013.

Whitley, R. J., Macinnis-Ng, C. M. O., Hutley, L. B., Beringer, J., Zeppel, M., Williams, M., Taylor, D., and Eamus, D.: Is productivity of mesic savannas light limited or water limited? Results of a simulation study, Glob. Change Biol., 17, 3130–3149, 2011.

Williams, R., Gill, A., and Moore, P.: Seasonal Changes in Fire Behaviour in a Tropical Savanna in Northern Australia, Int. J. Wildland Fire, 8, 227–239, 1998.

Williams, R. J., Duff, G. A., Bowman, D., and Cook, G. D.: Variation in the composition and structure of tropical savannas as a function of rainfall and soil texture along a large-scale climatic gradient in the Northern Territory, Australia, J. Biogeogr., 23, 747–756, 1996.

Wright, I. J., Westoby, M., and Reich, P. B.: Convergence towards higher leaf mass per area in dry and nutrient-poor habitats has different consequences for leaf life span, J. Ecol., 90, 534–543, 2002.

Zhu, Z., Bi, J., Pan, Y., Ganguly, S., Anav, A., Xu, L., Samanta, A., Piao, S., Nemani, R. R., and Myneni, R. B.: Global data sets of vegetation leaf area index (LAI) 3g and Fraction of Photosynthetically Active Radiation (FPAR) 3g derived from Global Inventory Modeling and Mapping Studies (GIMMS) Normalized Difference Vegetation Index (NDVI3g) for the period 1981 to 2011, Remote Sens., 5, 927–948, 2013.

Table 1. Model parameters.

Parameter	units	Value	Meaning	Equation	Source
θ_{S_1}	[$m^3 m^{-3}$]	Spatially variable	Saturated volumetric Water content (upper soil layer)	(1)	Sect. 3.1
θ_{S_2}	[$m^3 m^{-3}$]	Spatially variable	Saturated volumetric Water content (lower soil layer)	(1)	Sect. 3.1
Z_{W_1}	[m]	0.2	Depth of upper soil layer	(1)	This work (fixed)
Z_{W_2}	[m]	4.0	Depth of lower soil layer	(1)	This work (fixed)
c_{PT}	[ ]	1.26	Priestley–Taylor Coeffcient	(6)	Priestley and Taylor (1972)
G_a	[$m s^{-1}$]	0.015	Aerodynamic Conductance	(1.8)	This work (fixed)
$p_{extract}$	[ ]	0.421	Exponent in root water extraction	(11)	This work (calibrated)
$k_{E,g}$	[$m d^{-1}$ (mol C m^{-2})$^{-1}$]	6.14×10^{-4}	Rate constant for root water extraction (grass)	(11)	This work (calibrated)
$k_{E,w}$	[$m d^{-1}$ (mol C m^{-2})$^{-1}$]	6.12×10^{-4}	Rate constant for root water extraction (trees)	(11)	This work (calibrated)
β	[ ]	8.88	exponent specifying the response of soil evaporation to upper-layer soil water	(12)	This work (calibrated)
g	[ ]	1.30	exponent specifying the response of drainage to relative soil water	(14)	This work (calibrated)
K_{S_1}	[$m d^{-1}$]	Spatially variable	saturated hydraulic conductivity of soil layer 1	(14)	See Sect. 3.1
K_{S_2}	[$m d^{-1}$]	Spatially variable	saturated hydraulic conductivity of soil layer 2	(14)	See Sect. 3.1
$k_{L,g}$	[d^{-1}]	1/67	first order rate constant for leaf turnover (grass)	(15)	This work (calibrated)
$k_{R,g}$	[d^{-1}]	$k_{L,g}$	first order rate constant for fine root turnover (grass)	(15)	Janos et al. (2008)
$k_{R,w}$	[d^{-1}]	1/256	first order rate constant for fine root turnover (trees)	(15)	Vogt et al. (1995)
b_{growth}	[ ]	6.17	growth scaling parameter	(19)	This work (calibrated)
$F_{0,growth}$	[mol C $m^{-2} d^{-1}$]	0.017	residual growth flux to allow for regeneration from seed or resprouting	(19)	This work (calibrated)
k_{store}	[ ]	10.0	parameter controlling contribution of flux to NSC store to growth rate	(19)	This work (fixed)
p_{growth}	[ ]	3.0	parameter controlling steepness of soil moisture function used in growth formulation	(20)	This work (fixed)
w_{thresh}	[ ]	0.362	Relative soil moisture threshold in soil moisture function used in growth formulation	(20)	This work (calibrated)
K_{growth}	[ ]	0.02	scaling parameter controlling rate of change of the dynamic carrying capacity.	(21)	This work (fixed)
C_0	[mol C m^{-2}]	0.001	minimum carrying capacity	(21)	This work (fixed)
c_{growth}	[ ]	0.2	Growth respiration coefficient	(22)	Ryan (1991)
α_Q	[mol C mol quanta^{-1}]	0.0198	PAR use efficiency (trees and grass)	(24)	This work (calibrated)
$m_{\sigma,g}$	[ ]	1.5 $m_{\sigma,w}$	Dimensionless multiplier in equation for water use efficiency, grass	(24)	Singh and Misra (1985)
$m_{\sigma,w}$	[ ]	0.493	Dimensionless multiplier in equation for water use efficiency, trees	(24)	This work (calibrated)
k_{resp}	[d^{-1}]	0.0548	rate constant for maintenance respiration	(28)	Sprugel et al. (1995)
$ratio_{CtoN,\ sapwood}$	[g C (g N)$^{-1}$]	300	Carbon to nitrogen mass ratio in sapwood	(28)	Sitch et al. (2003)
$ratio_{CtoN,\ leaf}$	[g C (g N)$^{-1}$]	30	Carbon to nitrogen mass ratio in leaves	(28)	Sitch et al. (2003)
$ratio_{CtoN,\ roots}$	[g C (g N)$^{-1}$]	30	Carbon to nitrogen mass ratio in fine roots	(28)	Sitch et al. (2003)
$k_{LA:SA}$	[ ]	3000	Ratio of leaf area to sapwood cross-sectional area	(33)	McDowell et al. (2002)
c_{Ext}	[ ]	0.6	Extinction coefficient for PAR	(34)	This work (fixed)
$A_{SL,g}$	[cm^2 g (DW)$^{-1}$]	120.0	Specific Leaf Area, grass	(37)	Lower than the recommended values of 175 (Hutley, pers comm) to account for clumping

Table 2. Locations and characteristics of OzFlux sites (after Hutley et al., 2011).

Site	Coordinates	Reference	Ecosystem	Dominant vegetation	Data period
1. Howard Springs (HS)	12.4952° S 131.1501° E	(Beringer et al., 2003, 2011)	Open-forest savanna	*Eucalyptus miniata* and *E. tetrodonta*, *Sorghum intrans, S. plumosum Heteropogon triticeus* grassy understorey	Jan 2001–Dec 2013
2. Adelaide River (AR)	13.0769° S 131.1178° E	Beringer et al. (2007) Beringer et al. (2011)	Open-forest savanna	*E. tectifica, Planchonia careya, Buchanania obovata woodland savanna, Sorghum spp., Chrysopogon falla grassy understory*	Jan 2007–May 2009
3. Daly R Savanna (DR)	14.1592° S 131.3833° E	Beringer et al. (2011)	Woodland savanna	*E. tetrodonta, C. latifolia, Terminalia grandiflora Sorghum sp.* and *H. triticeus*	Jan 2007–Dec 2013
4. Dry Creek (DC)	15.2588° S 132.3706° E	Beringer et al. (2011)	Woodland savanna	*E. tetrodonta, E. dichromophloia, C. terminalis, S. intrans, S. plumosum, Themeda triandra* and *C. fallax*	Jan 2010–Jun 2013
5. Alice Springs (AS)	22.283° S 133.249° E	Cleverly et al. (2013)	Acacia woodland	*Acacia aneura*	09/2010–Dec 2013

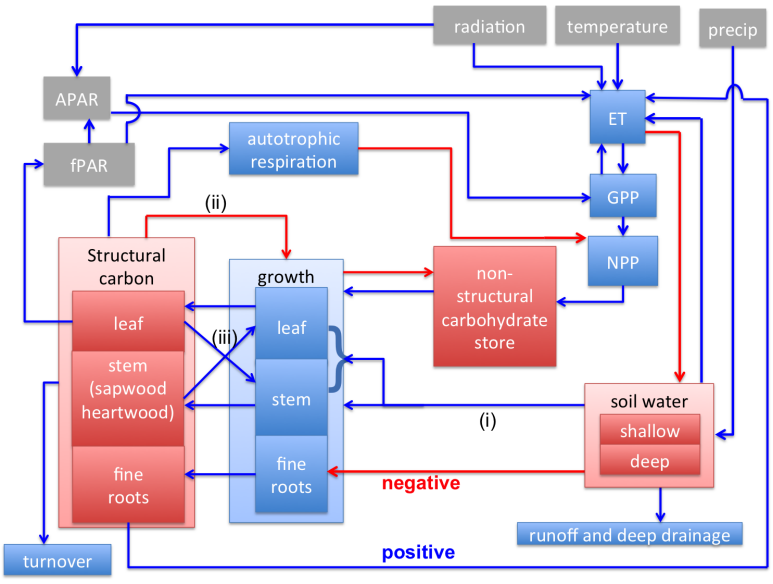

Figure 1. Schematic showing the key elements of HAVANA, and the qualitative relationships between them. Carbon and water pools are represented by red boxes; fluxes by blue boxes. Blue (red) arrows show positive (negative) feed-backs. Less intuitive feed-backs are: (i) Soil water influence on growth: soil water positively impacts on total growth, while there is a negative feed-back of soil moisture on allocation to fine roots, in favour of the combined (leaf + stem) compartment; (ii) Growth responds negatively to the structural carbon store as it approaches carbon carrying capacity (Eq. 19); (iii) Partitioning of growth between leaf and stem is influenced by the relative magnitudes of leaf and sapwood compartments, which are constrained by the Pipe Model (Shinozaki et al., 1964), in which sapwood cross-sectional area is assumed to be a constant proportion of total leaf area.

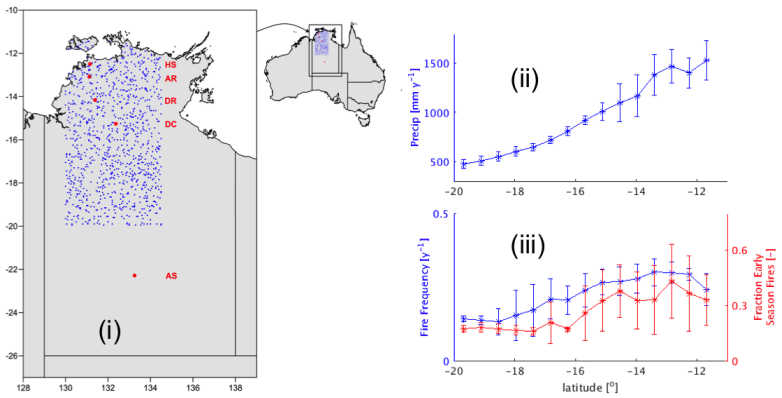

Figure 2. (i) Map of 1000 points representative of the study area, and locations of flux sites (red dots) for use in calibration/validation; (ii) latitudinal variation of mean annual precipitation (1900–2013) and (ii) latitudinal variation of fire frequency and fraction of fires occurring in the early part of the dry season (pre-August) (1989–2011). Each point represents a spatial average across ~ 65 points lying within a latitude bin of width 0.57°, with error bars representing one standard deviation.

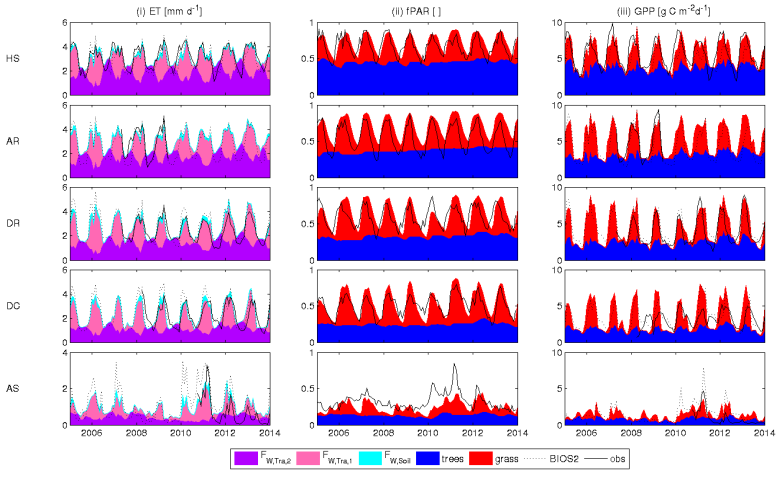

Figure 3. Monthly (2005–2013) time-series of (i) ET, (ii) fPAR and (iii) GPP at five flux stations: HAVANA-POP (stacked plots); BIOS2 (full biogeochemical model with prescribed vegetation cover) and observations. HAVANA-POP ET is partitioned into soil evaporation and transpiration from each of the upper (1) and lower (2) soil layers. HAVANA-POP fPAR and GPP are partitioned into tree and grass components. Flux site abbreviations (left of figure) are given in Table 2.

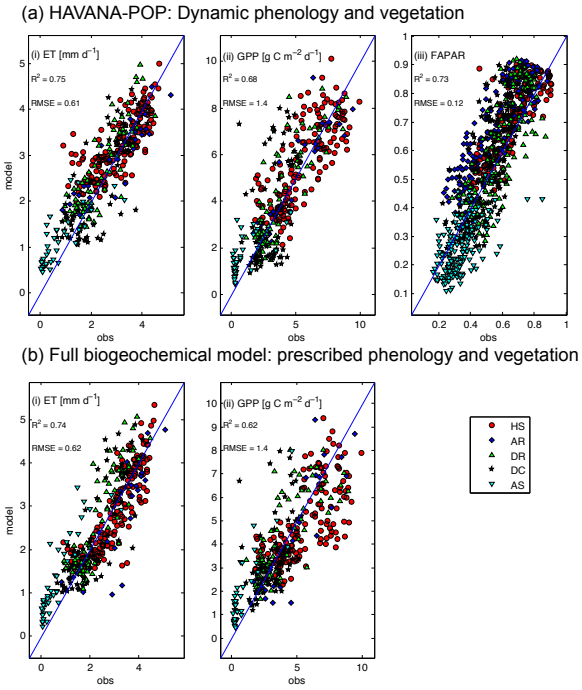

Figure 4. Scattergrams of model predictions vs. observations of monthly values at 5 Flux Sites of (i) ET; (ii) GPP; (iii) fPAR. **(a)** HAVANA-POP and **(b)** CABLE in BIOS2, a full biogeochemical model with prescribed phenology and vegetation cover.

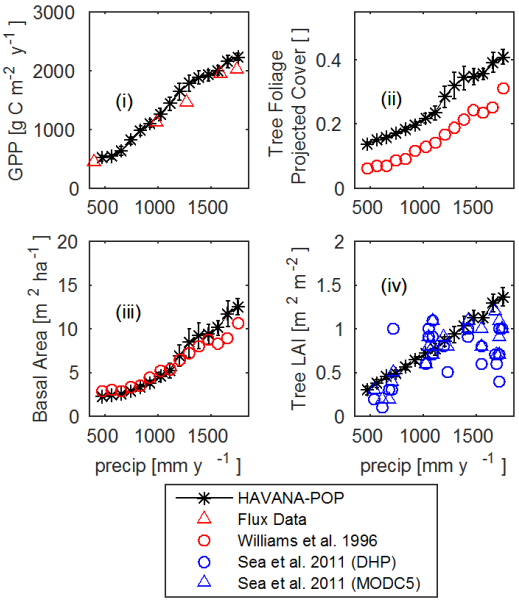

Figure 5. Time-averaged (1964–2013) HAVANA-POP output variables: variation with rainfall and comparison with observation-based estimates. (i) Gross primary production (combined tree and grass components) and comparison with mean annual GPP from flux data (averaged over observation period); (ii) Annual average tree foliage projected cover and comparison with Williams et al. (1996); (iii) tree basal area and comparison with Williams et al. [1996]; (iv) Dry season tree LAI (September 2008) and comparison with Sea et al. (2011) estimated from digital hemispheric photography (DHP) and the MODIS Collection 5 product (MODC5).

Discussion Paper | Discussion Paper | Discussion Paper | Discussion Paper |

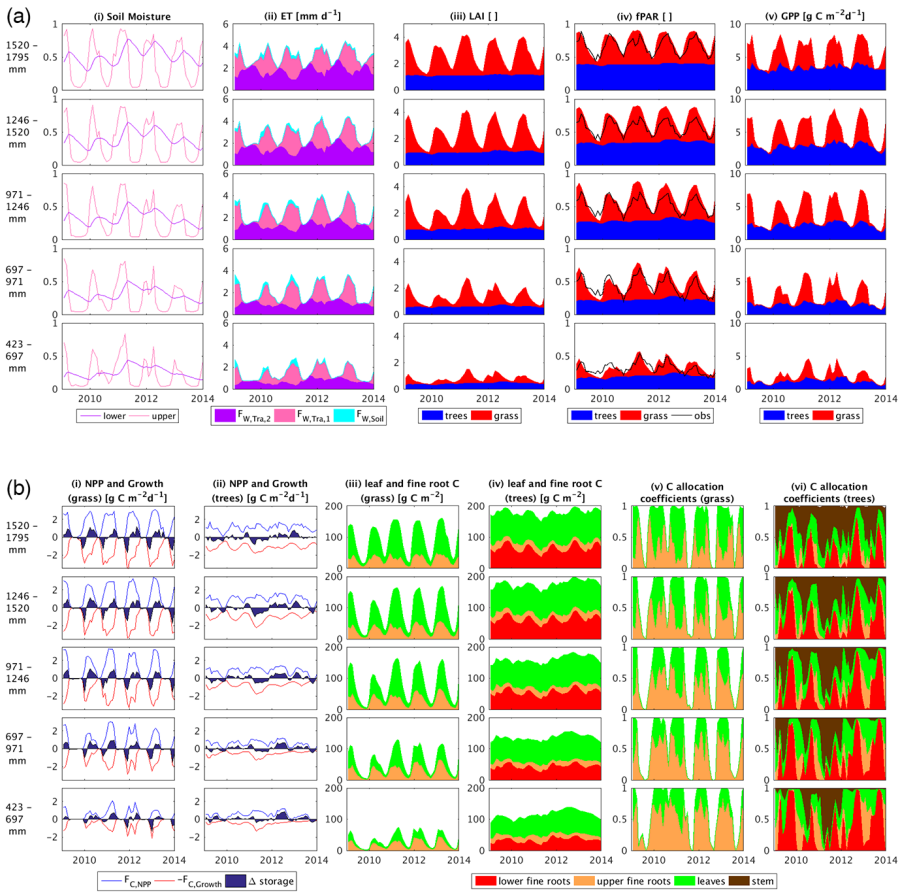

Figure 6. (a) Monthly time series (2009–2014) of (i) soil moisture (w_1 and w_2); (ii) ET; (iii) leaf area index (LAI) (iv) FPAR and (v) GPP, as predicted by HAVANA-POP. Corresponding observed FPAR is also shown. Each row represents a spatial average over the randomly sampled gridcells (Fig. 2i) falling within the range of mean annual precipitation shown on the left. **(b)** Monthly mean time series (2009–2014) of (i) NPP, growth and change in storage (grass); (ii) NPP, growth and change in storage (trees); (iii) leaf and fine root carbon pools (grass); (iv) leaf and fine root carbon pools (trees); (v) C allocation coefficients to leaves and fine roots (grass); (vi) C allocation coefficients to leaves, fine roots and stems (trees). Spatial aggregation is the same as in **(a)**.

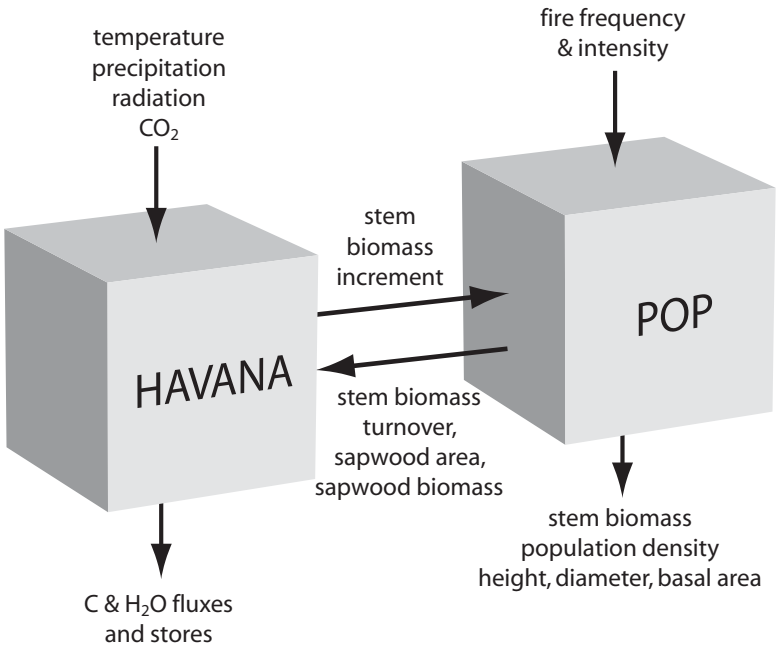

Figure A1. HAVANA-POP coupling.